Hindawi
Advances in Civil Engineering
Volume 2019, Article ID 7891948, 15 pages
https://doi.org/10.1155/2019/7891948

Research Article

Dynamic Property of a New Type of Postearthquake Temporary Prefabricated Lightweight Steel Structure

GuoQi Xing,[1] **Qing-hai Li**,[2] **JingJie Yu**,[1] **and Wei Xuan**[1]

[1]*College of Civil Engineering and Architecture, Weifang University, Weifang 261061, China*
[2]*China Building Materials Academy, Beijing 100024, China*

Correspondence should be addressed to GuoQi Xing; xgq1105@163.com

Received 14 October 2018; Revised 29 December 2018; Accepted 10 January 2019; Published 14 February 2019

Academic Editor: Raffaele Landolfo

For a new type of postearthquake temporary prefabricated lightweight steel structure proposed in this paper, mainly composed of steel frame, prefabricated hanger slabs, prefabricated hanger columns, reinforced concrete superposed slabs, etc., parameters of dynamic property for the structure, including natural frequency, vibration mode, damping ratio, etc., are determined by the test method. For prefabricated hanger columns and prefabricated hanger slabs, they are all produced with construction waste in factory and assembled on-site, which can form exterior walls. The united method, based on forced vibration method and ambient random vibration method, can quickly obtain accurate natural frequencies of the full-scale two-story experimental model. In this paper, damping oscillatory method is used to obtain damping ratio which can be determined only by the test method. In order to analyse the modal of the experimental model, a finite element model for the full-scale two-story experimental model is established, where the weight of prefabricated hanger slabs is assumed to be supported by prefabricated hanger columns, and the stiffness of prefabricated hanger columns is also increased. In addition, the connections between lightweight steel frame and prefabricated hanger columns are regarded as flexible connection. Comparing natural frequencies obtained from the finite element method with that obtained from the test method, magnification factor of stiffness for prefabricated hanger column is determined. In the analysis of modal for the full-scale two-story experimental model, the results show that the experimental model satisfies the requirement of design for seismic performance.

1. Introduction

Prefabricated lightweight steel structures, which are fabricated in factor and assembled on-site, have many advantages, such as relatively better construction quality, faster construction speed, and so on [1], belonging to environmentally friendly building practices [2]. Therefore, the structure is often applied to the rural residencies. Due to the lightweight of the structure, it has good seismic performance and is especially suitable for high seismic zones [3]. In order to make use of the construction waste produced after the earthquake, a new type of postearthquake temporary prefabricated lightweight steel structure is proposed in this paper. The structure is different from other lightweight steel structure, composed of steel frame (Figure 1(a)), prefabricated hanger columns and prefabricated hanger slabs (Figure 1(b)), and reinforced concrete superposed slab (Figure 2). For the prefabricated hanger column and prefabricated hanger slab, they are all produced with construction waste in factory and assembled on-site.

For the conventional lightweight steel structure, Xu et al. [3] investigated the dynamic characteristic of prefabricated houses and got the natural frequencies, damping ratios, and vibrational modes for the structure. In addition, some scholars were focused on the performance of joints existing in the conventional lightweight steel structure subjected to earthquake action, such as traditional welded joints [4–6], dog bone joints [7], and joints with long grooves and enlarged welding holes [8, 9]. Goel et al. [10] conducted an experimental study and theoretical analysis for a joint with a girder web opening. Moreover, the static properties and seismic performances of T-stub bolted connections were

(a) (b)

Figure 1: Prefabricated lightweight steel structure. (a) Steel frame. (b) Exterior walls: (i) prefabricated hanger slab and (ii) prefabricated hanger column.

(a) (b)

Figure 2: Sketch of floorslab. (a) Floorslab: (i) hot-rolled equilateral angle steel and (ii) reinforced concrete superposed slab. (b) Fine aggregate concrete.

investigated with model experiments and finite element analysis [11–15]. Many other scholars proposed new beam-to-column joints with good seismic performance and carried out seismic tests and finite element analysis on them [16–19].

For the new type of postearthquake temporary prefabricated lightweight steel structure to be widely used in the rural residencies especially situated in high seismic zones, the seismic performance of the structure should be investigated. Before investigating the seismic performance of the structure, the dynamic properties, including natural frequency, vibration mode, damping ratio, etc., should be first studied with experiment method and the finite element method in this paper. Therefore, the research on dynamic properties of the structure can provide basis for the subsequent research on seismic performance in the future.

Figure 3: Full-scale two-story experimental model: (i) ground beam and (ii) prefabricated lightweight steel structure.

2. Experimental Model and Testing System

2.1. Experimental Model. To accurately obtain the dynamic properties of the new type of prefabricated lightweight steel structure, a full-scale two-story experimental model is built (Figure 3). Considering the dimension of shake table used in test of seismic performance, the dimension of the experimental model in the plane is 2400 mm in length and 2400 mm in width (Figures 2(a) and 2(b)). Besides, the height of the story is 2650 mm (Figure 4(c)). Sloping roof is used in the experimental model and is placed on steel roof truss, of which the slope is about 34° and the height is 800 mm. In the experimental model, there are two openings in walls on the second floor, which represent windows whose dimension is 1200 mm in width and 1650 mm in height. And on the first floor, two openings in walls also exist, which represent doors whose dimension is 1200 mm in width and 2000 mm in height. The experimental model is fixed with the steel plate whose thickness is 20 mm according to welding

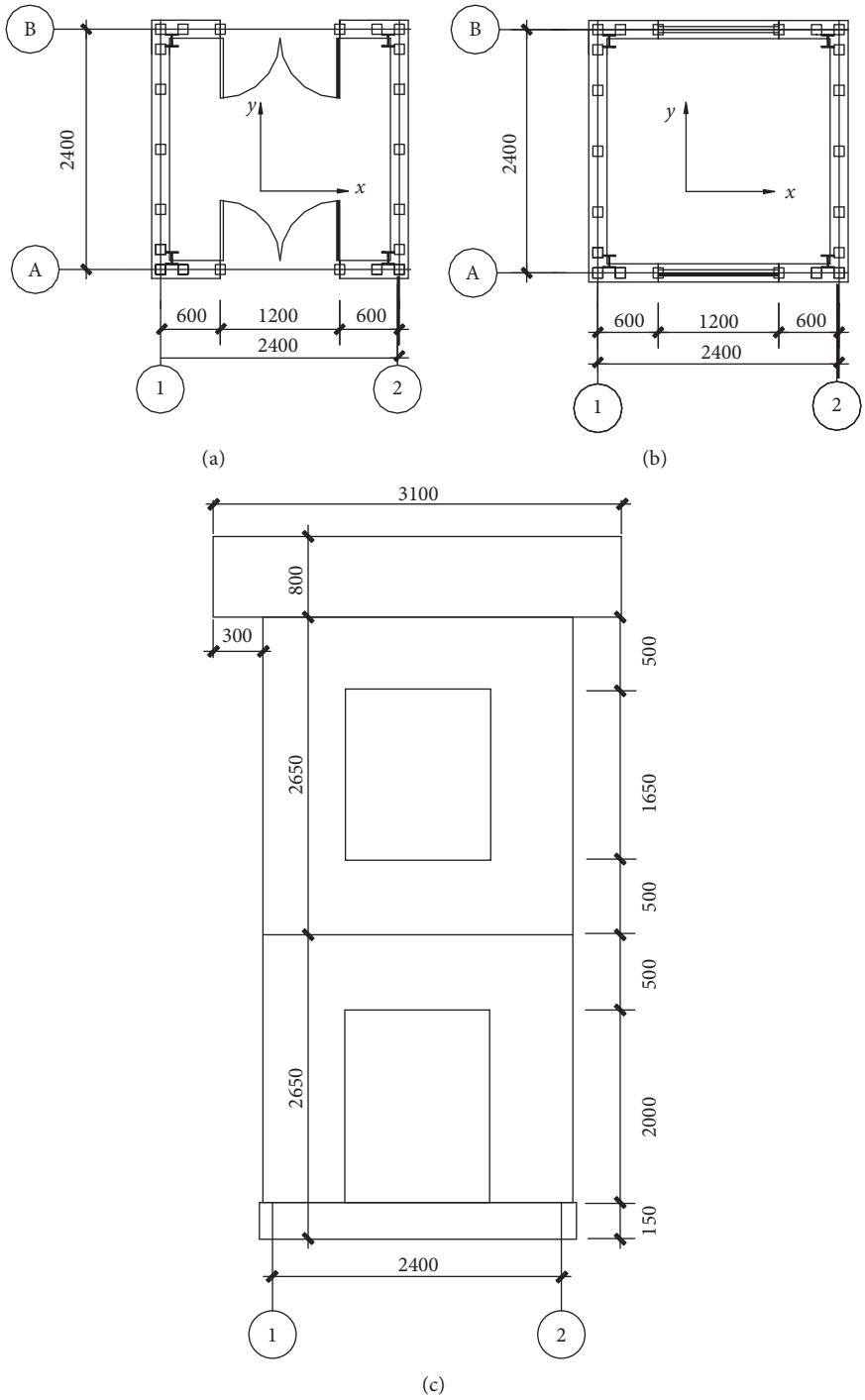

Figure 4: The detailed dimension of experimental model. (a) Plan for first floor. (b) Plan for second floor. (c) Elevation for experimental model. Unit: mm.

the columns with steel plate. For the steel plate whose dimension is 2600 mm in length and 2600 mm in width, it is fixed on the ground according to bolted connection.

In the experimental model, the column (5600 mm in length) is a hot-rolled H-shaped steel column (HW 125 × 125 × 6.5 × 9.0 mm) and the beam (1950 mm in length) is also a hot-rolled H-shaped steel beam (HW 125 × 125 × 6.5 × 9.0 mm). The columns and beams can be assembled by welding on-site, which use Q235B steel (yield stress value and ultimate stress value are 235 MPa and 355 MPa, respectively). In order to make the columns firmly embedded in ground beams whose dimension is 150 mm in height and 120 mm in width, four flanges shaped like triangle are welded with column at the bottom of each column. When the steel frame is finished, hot-rolled equilateral angle steel (∠40 × 40 × 5 mm) is used as secondary beam, which also

uses Q235B steel, connecting with beams by welding (Figure 4(a)). Reinforced concrete superposed slab (Figure 4(a)) with 60 mm in thickness is placed on the secondary beams, connecting with beams by welding. In order to make all slabs form one whole, fine aggregate concrete (Figure 4(b)) with 30 mm in thickness is poured on the surface of reinforced concrete superposed slabs.

Prefabricated hanger columns with a distance of 600 mm are fixed with the beams by semirigid connection, whose dimension is 100 mm in width and 100 mm thickness, with 2000 Kg/m^3 in density. In order to improve the strength of prefabricated hanger columns, steel bar with 16 mm in diameter is placed in them, as shown in Figure 5(a). In addition, in order to support prefabricated hanger slab, the hanger should be set on prefabricated hanger column, as shown in Figure 5(b). However, considering the complexity of force acting on the prefabricated hanger column at the corners, the spacing of prefabricated hanger columns near the corners should be reduced to 300 mm. When the installing of prefabricated hanger columns is finished, prefabricated hanger slabs with 2100 Kg/m^3 in density are placed on prefabricated hanger columns, which are perpendicular to the prefabricated hanger columns. For prefabricated hanger slabs, the dimension is 180 mm in width and 40 mm thickness, as shown in Figure 6. In order to improve the strength of prefabricated hanger slab, steel wires with 2 mm in diameter are placed in them. In the experimental model, prefabricated hanger slabs with 600 mm length and 1200 mm length are used. According to the connection between prefabricated hanger slab and prefabricated hanger column, which is shown in Figure 7, all prefabricated hanger slabs and prefabricated hanger columns can form exterior walls. Besides, in the experimental model, the lintel should be placed at bottom and top of the windows and at the top of doors, whose dimension is 1200 mm in length, 80 mm in width, and 40 mm thickness.

In order to make the exterior walls meet the requirement of heat preservation, firstly, expanded polystyrene foam board with 16 kg/m^3 in density and 20 mm thickness is pasted on the inner surface of the exterior wall. And then the mineral wool board with 100 mm thickness is pasted on the surface of expanded polystyrene foam board. In addition, thermal insulation board with 30 mm thickness is pasted on the surface of mineral wool board.

Moreover, for the sloping roof, it is placed on the roof truss made of hot-rolled steel channel ($100 \times 48 \times 5.3$ mm), which uses Q235B steel. Roof slab (Figure 8) with thermal insulating layer is placed on the roof truss, whose thickness is 60 mm. In order to simulate live load imposed on the surface of floorslab, the weight of 5.76 kN is placed on the surface of floorslab on the second floor (Figure 9(a)). For the live load imposed on roofing, the weight of 1.73 kN is placed on the roof truss (Figure 9(b)). The total weight of the experimental model is about 117.6 kN.

2.2. Arrangement of Acceleration Transducers. In the test of dynamic property, acceleration transducers (Figure 10) can be used to obtain the curve of damping oscillatory and resonance curve [20]. Based on the curve of damping oscillatory and resonance curve, natural frequencies, vibration mode, and damping ratio can be determined further.

Due to the symmetry of the experimental model, torsional vibration cannot be considered in the test. Therefore, the translational vibration is only considered in the test, and acceleration transducers should be placed on the symmetrical axis of plane of the experimental model. For the bottom of the first floor, acceleration transducers should be placed on the ground beams near the exterior walls. In addition, the direction of vibration on the symmetrical axes of plan of the experimental model, measured by acceleration transducers, should be perpendicular to each other, as shown in Figure 11(a). The acceleration transducers situated on the floorslab of the second floor, which are near the exterior walls, should also be placed on the symmetrical axis of plane of the experimental model, as shown in Figure 11(b). The acceleration transducers situated on the top of the second floor should be placed on the beams where the roof trusses are placed, as shown in Figure 11(c).

2.3. Experiment Method. The forced vibration method and ambient random vibration method are often used to obtain the natural frequencies [21]. In the test of dynamic property, in order to quickly obtain accurate natural frequencies of the experimental model, the united method is adopted. Firstly, the ambient random vibration method is used in the test, and fluctuating signals can be determined based on acceleration transducers placed on the model and signal collector (Figure 12(a)), as shown in Figure 12(b).

Based on the peak value of fluctuating signals, the approximate natural frequencies can be determined. Next, the forced vibration method is used to obtain accurate natural frequencies of the model. In forced vibration method, the natural frequencies obtained from ambient random vibration method are input to signal generator which can make vibration exciter vibrate and also can make the structure vibrate and are adjusted to make the structure resonate. The detailed process is shown in Figure 13.

In this paper, the vibration exciters are placed on the beams situated on the top of first floor and second floor, as shown in Figure 14(a). Moreover, all the vibration exciters are placed on the symmetrical axis of plan of the experimental model, as shown in Figures 14(b) and 14(c).

In test of dynamic property, when the experimental model resonates, excited by vibration exciter under natural frequencies, the resonance curve for the experimental model can be received by acceleration transducer. By means of the resonance curve, the mode of vibration can be further obtained. In order to obtain the curve of damping oscillatory received by acceleration transducers, vibration exciters are shut off when the experimental model resonates. By means of curve of damping oscillatory, damping ratio obtained only by the test method can be determined.

3. Analysis of Experiment Results

3.1. Analysis of Natural Frequency. If fluctuating signal is assumed to be stationary white noise with band-limited,

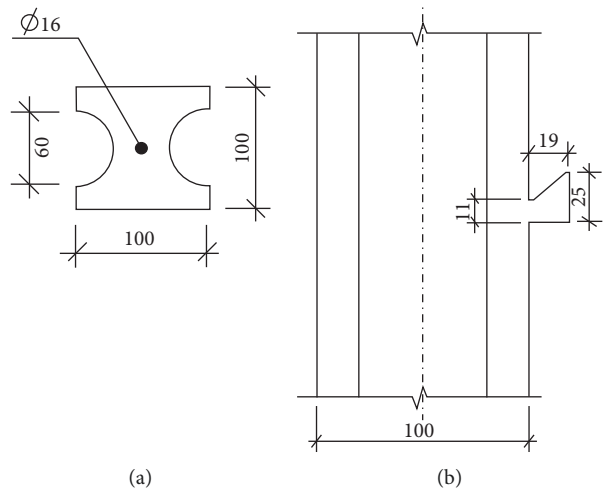

Figure 5: Sketch of prefabricated hanger column. (a) The dimension of prefabricated hanger column. (b) The dimension of hanger on prefabricated hanger column. Unit: mm.

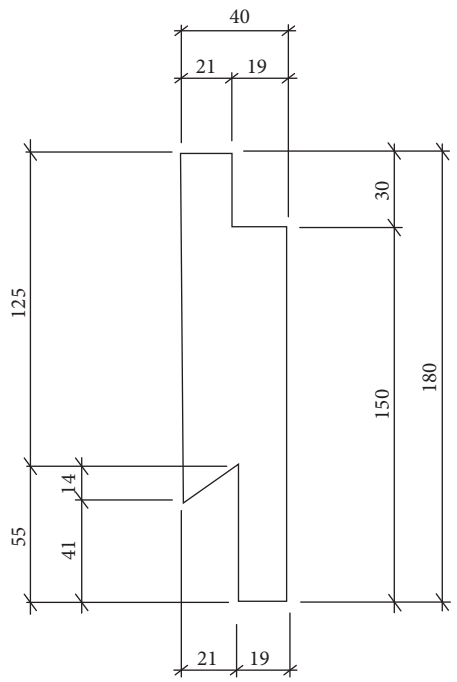

Figure 6: Sketch of prefabricated hanger slab. Unit: mm.

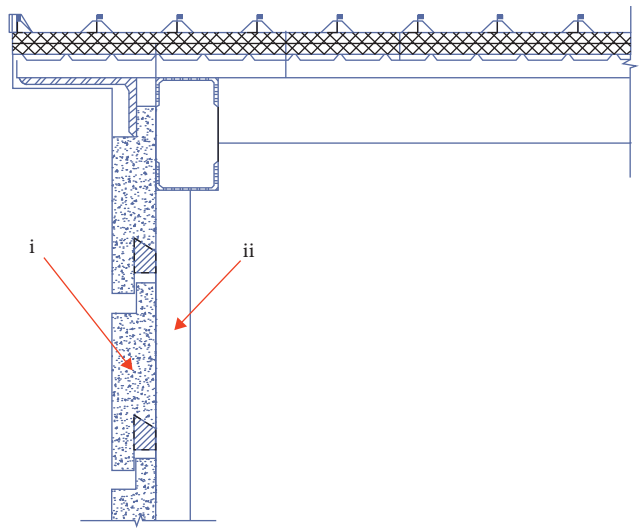

Figure 7: Connection between (i) prefabricated hanger slab and (ii) prefabricated hanger column.

power spectrum for fluctuating signal is constant [22]. In this condition, for the experimental model, frequency spectrum of transfer function is consistent with that of fluctuating signal. Therefore, natural frequency is only related to auto-power spectrum and cross-power spectrum of fluctuating signal. Due to the existence of noise generated during test and the influence of vibration exciter, the peak value of auto-power spectrum for fluctuating signal may not be natural frequency. In order to obtain the accurate natural frequencies for the experimental model, the following should be considered based on auto-power spectrums and cross-power spectrums of fluctuating signals [22]:

Figure 8: Installing roof slab. Aluminium plate with 1.5 mm thickness is pasted on the surface of roof slab, and slab joints as well as lap joint are filled with polyurethane foamable adhesive.

(a) (b)

Figure 9: Simulating live load. (a) At floorslab of second floor. (b) At roof truss.

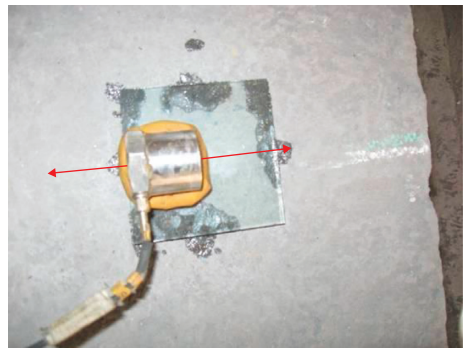

Figure 10: Acceleration transducer. The arrows indicate the direction of vibration which can be measured by acceleration transducer.

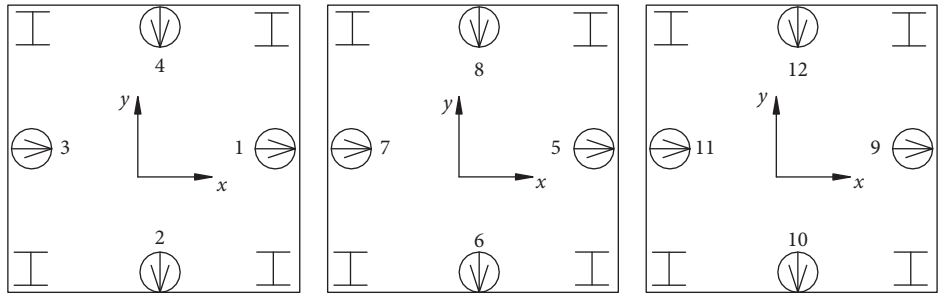

(a) (b) (c)

Figure 11: Arrangement of acceleration transducers. (a) At bottom of first floor. (b) At bottom of second floor. (c) At top of second floor.

(1) Peak values of auto-power spectrums for fluctuating signals obtained from all acceleration transducers placed on the experiment model are all approximately equal.

(2) When the experimental model resonates, the values of coherence function for fluctuating signals obtained from all acceleration transducers are maximum.

(3) When the experimental model resonates, phase angles for fluctuating signals obtained from all acceleration transducers placed on experiment model are all approximately equal or the difference between phase angles is about 180°.

Based on auto-power spectrums for fluctuating signal obtained from all acceleration transducers placed on the experimental model and cross-power spectrums for fluctuating signals obtained from acceleration transducer notated 1 and 2, natural frequencies of the experimental model in X direction can be determined with the ambient random vibration method, as shown in Figures 15(a) and 15(b). Natural frequencies in Y direction can also be determined with the same method mentioned above, as shown in Figures 15(c) and 15(d).

Based on the natural frequencies obtained with ambient random vibration method, the accurate natural frequencies of the experimental model in X direction can be determined with the forced vibration method, in the process mentioned

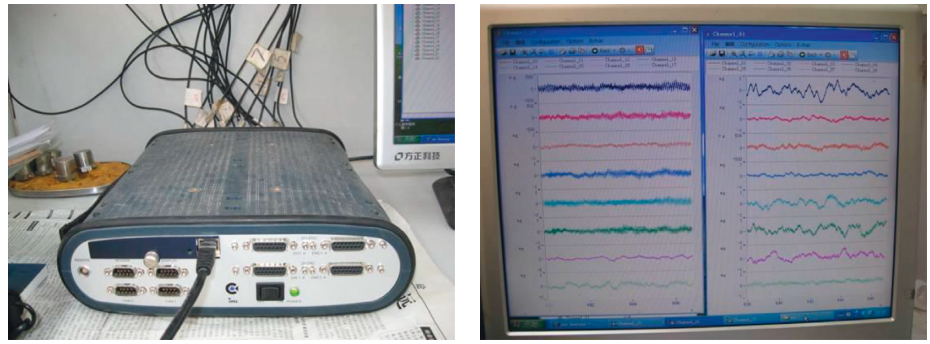

(a) (b)

Figure 12: Collecting fluctuating signals. (a) Signal collector. (b) Fluctuating signals.

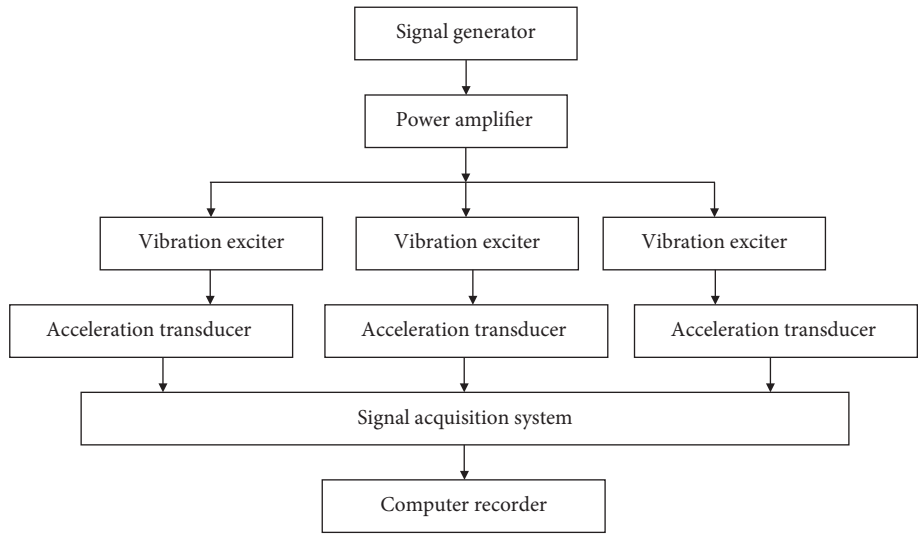

Figure 13: Process of dynamic property test with forced vibration method.

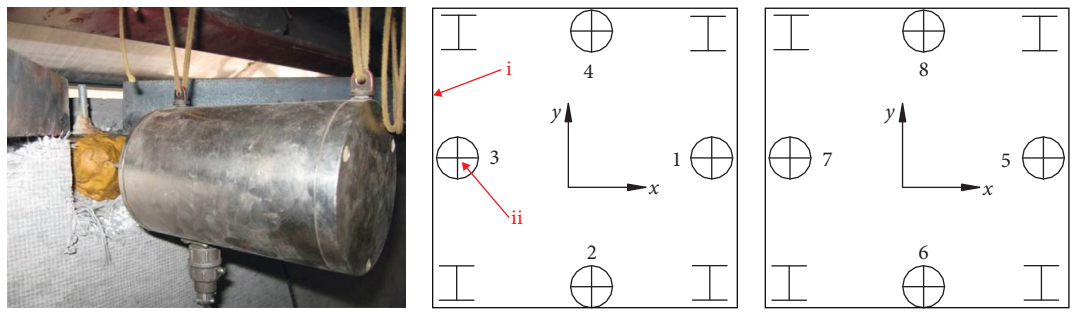

(a) (b) (c)

Figure 14: Arrangement of vibration exciter. (a) Vibration exciter. (b) On top of first floor: (i) beam and (ii) acceleration transducer. (c) On top of second floor.

above, as shown in Figures 16(a) and 16(b). The natural frequencies of the experimental model in X direction can also be determined, as shown in Figures 16(c) and 16(d).

In order to compare the natural frequencies obtained with ambient random vibration method with those obtained with the forced vibration method, all natural frequencies are shown in Table 1. As can be seen from Table 1, natural frequencies obtained with the ambient random vibration method are approximately equal to that obtained with the forced vibration method, in X or Y direction, for the same vibration mode of the experimental model. In addition, it also shows that for first-order and second-order vibration

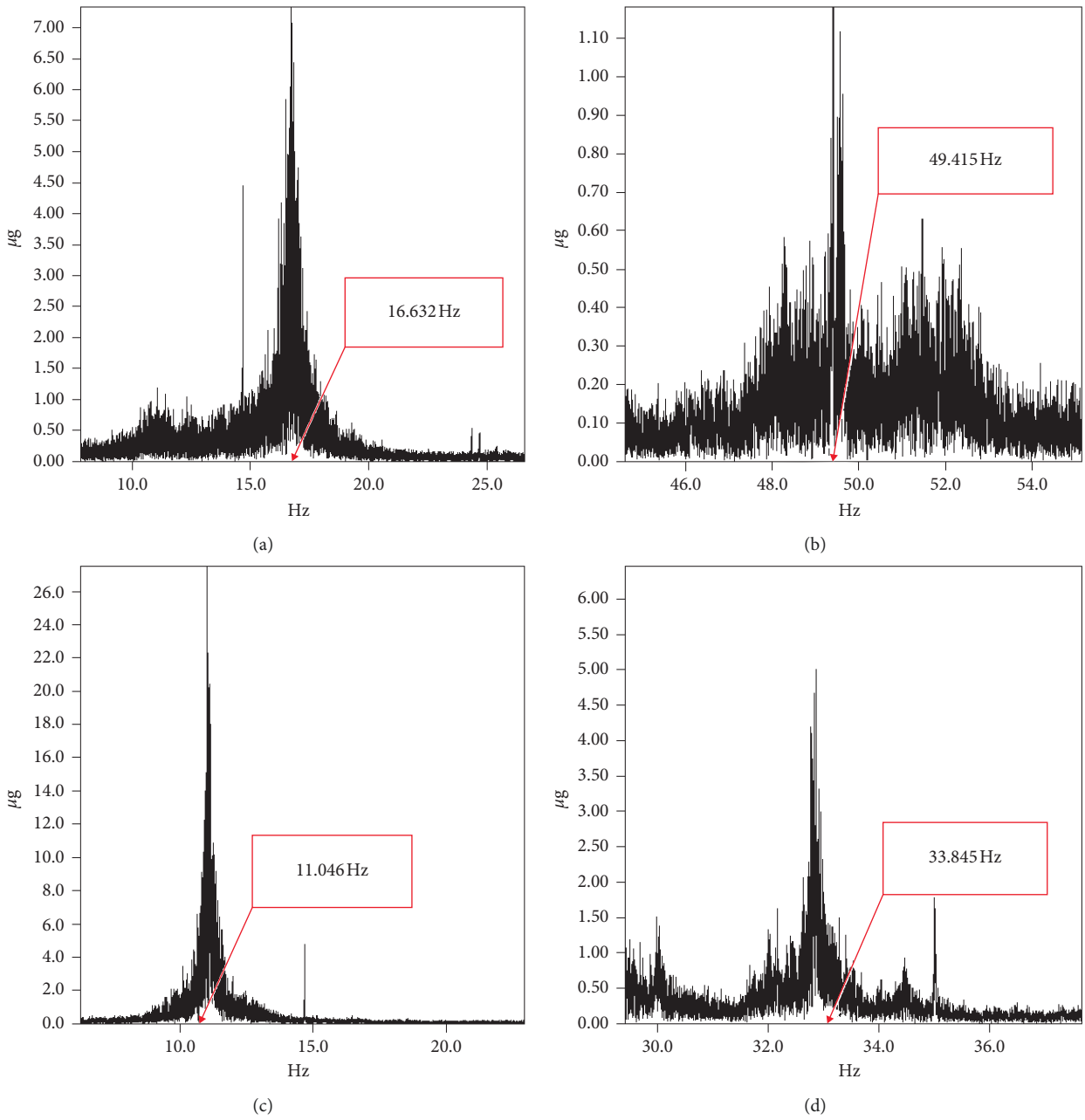

Figure 15: Natural frequencies obtained with the ambient random vibration method. (a) First order in X direction. (b) Second order in X direction. (c) First order in Y direction. (d) Second order in Y direction.

mode, natural frequencies in X direction are higher than that in Y direction. The reason is that the stiffness of the experimental model in X direction is larger than that in Y direction. As can be seen from Figure 3, the hole on the exterior wall parallel to X direction can reduce the stiffness of the experimental model, thus the stiffness of exterior wall parallel to Y direction is larger than that of the X direction.

3.2. Analysis of Vibration Mode. In test of dynamic property, when the experimental model resonates, based on the fast Fourier transformation of fluctuating signals obtained from acceleration transducers placed on the locations which are on the same vertical position of the experimental model, amplitude-frequency curves of frequency response function for acceleration transducers can be determined with the software of uTekMa which can record and analyse the fluctuating signals. Based on amplitude-frequency curves, the ratio of peak values of fluctuating signals obtained at the natural frequency can be determined, which is equal to the ratio of coordinate values of vibration mode at the same natural frequency. In addition, positive and negative sign of coordinate values can be determined according to the phase angles of cross-power spectrums for fluctuating signals obtained at the natural frequency. Therefore, the vibration modes at natural frequencies in X direction can be

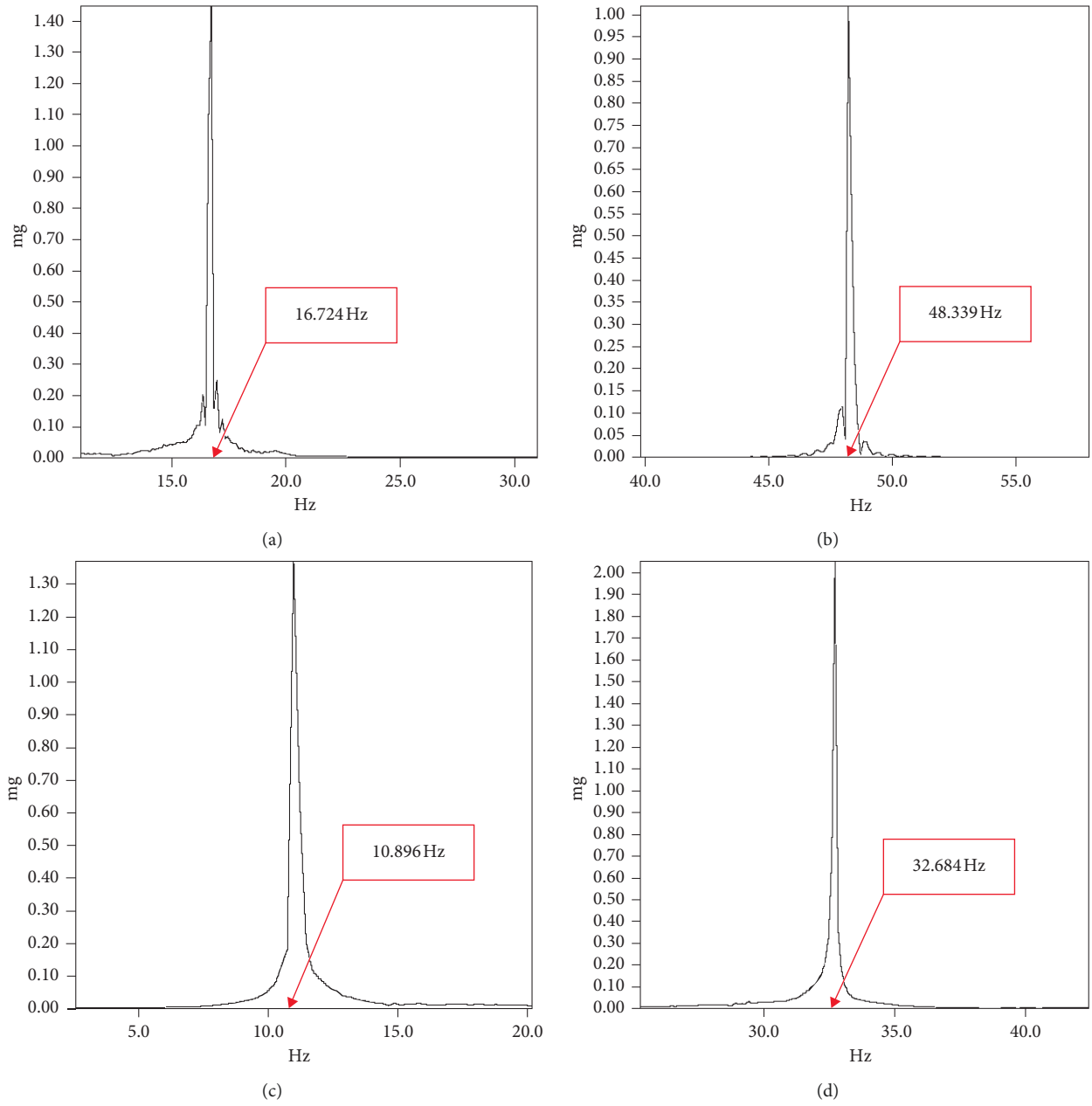

Figure 16: Natural frequency obtained with the forced vibration method. (a) First order in X direction. (b) Second order in X direction. (c) First order in Y direction. (d) Second order in Y direction.

Table 1: Natural frequencies obtained from two methods.

Vibration mode	Natural frequency in X direction (Hz)		Natural frequency in Y direction (Hz)	
	Ambient random vibration method	Forced vibration method	Ambient random vibration method	Forced vibration method
First-order	16.632	16.724	11.046	10.986
Second-order	49.415	48.339	33.845	32.684

determined based on the principle mentioned above, as shown in Figures 17(a) and 17(b). The vibration modes at natural frequencies in Y direction can also be determined, as shown in Figures 17(c) and 17(d).

As can be seen from Figures 17(a) and 17(c), the first-order vibration mode in X direction is similar to that in Y direction. For the second-order vibration mode in X direction, it is the same as that in Y direction, as shown in

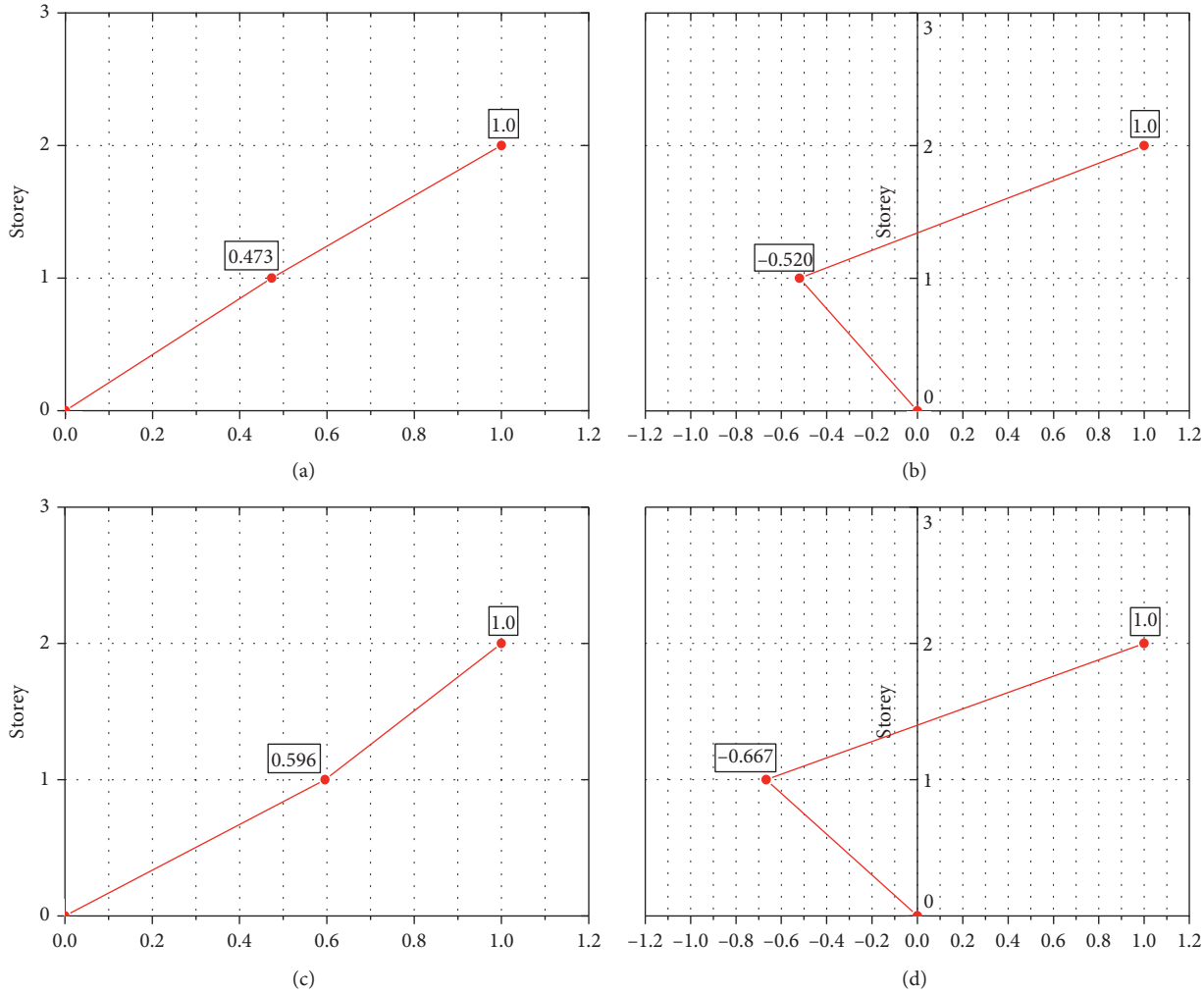

Figure 17: Vibration mode obtained with software uTekMa. (a) First order in X direction. (b) Second order in X direction. (c) First order in Y direction. (d) Second order in Y direction.

Figures 17(b) and 17(d), and the reason is due to the symmetry of the experimental model.

3.3. Analysis of Damping Ratio. Damping ratio of the experimental model can be determined only with the test method. Both the half-power point method and damping oscillatory method can be used to obtain damping ratio [23]. In this paper, the damping oscillatory method is used. When the experimental model resonates, vibration exciters are shut off, and then the curve of damping oscillatory (Figure 18) obtained from acceleration transducer can be recorded by the signal acquisition system. Moreover, the software of uTekMa can change the curve of damping oscillatory to the curve of amplitude oscillatory. Based on the curve of amplitude oscillatory, damping ratio can be further determined. In this paper, considering the existence of DC component in the curve of damping oscillatory, the following method is adopted to obtain the accurate damping ratio.

In Figure 19, $A_{\max(k)}$ and $A_{\max(k+n)}$ denote maximum amplitude in kth period and maximum amplitude in

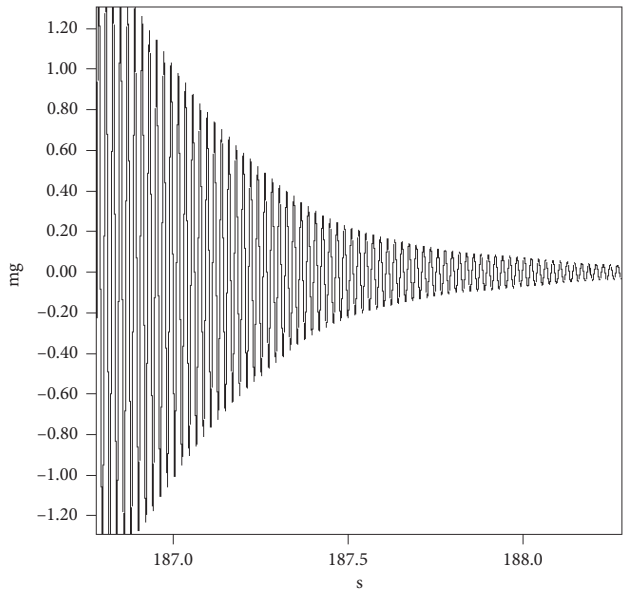

Figure 18: Curve of damping oscillatory.

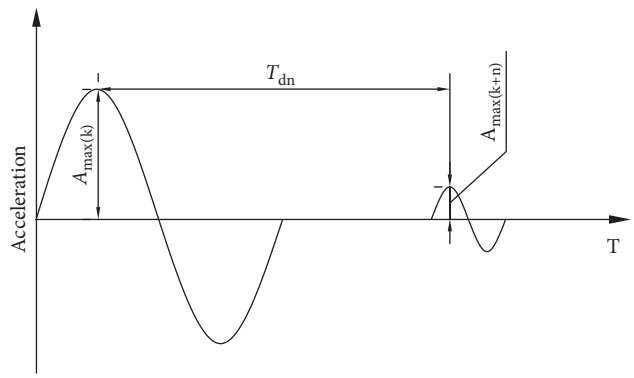

Figure 19: Curve of amplitude oscillatory. T_{dn} denotes the time between maximum amplitude in kth period and maximum amplitude in $(k+n)$th period.

$(k+n)$th period, respectively. Bao et al. [24] proposed that damping ratio ζ could be defined as

$$\zeta = \frac{1}{2\pi n} \cdot \ln \frac{A_{\max(k)}}{A_{\max(k+n)}}. \quad (1)$$

Based on the curve of amplitude oscillatory and equation (1), damping ratio in X and Y direction at different natural frequencies can be calculated with the method mentioned above, as shown in Table 2.

As can be seen from Table 2, for first-order vibration mode, damping ratio decreases with the increase of natural frequency. It can also be seen that for the first-order vibration mode, damping ratio in X and Y direction is 1.0397% and 1.2985%, respectively, which is less than allowable value of 5% required by China Code for Seismic Design of Building [24]. The reason that the damping ratios are very low is that, firstly, the form of constituting for exterior wall can reduce damping of the experimental model; secondly, the connections between steel frame and prefabricated hanger columns (semirigid connections) also can reduce damping. Moreover, the weight of exterior wall is light, and it can also make the damping ratio low. Therefore, the damping ratios in X and Y direction are very low.

4. Analysis of Finite Element Method

4.1. Finite Element Model. In this section, a finite element model is established with 3D software SAP2000, as shown in Figures 20(a) and 20(b). Exterior walls which are composed of prefabricated hanger columns and prefabricated hanger slabs are new type of walls, rather complicated compared to other walls. In addition, finite element for wall, including membrane element, shell element, plane element, etc., cannot be used to simulate the new type of wall. In the finite element model for the experimental model, exterior walls can be regarded as support of steel frame. Moreover, the weight of prefabricated hanger slabs is supported by prefabricated hanger columns, and it makes the stiffness of prefabricated hanger columns increase. Prefabricated hanger columns are supported by beams existing in the steel frame. In the finite element model, the connections between prefabricated hanger columns and beams existing in the steel frame are regarded as flexible connection. Besides, the weight of floorslab of second floor and live load imposed on the surface of floorslab of second floor are all regarded to be distributed on the beams situated on the bottom of second floor.

Table 2: Damping ratio of the experimental model (%).

	In X direction		In Y direction	
	$f_1 = 16.724$	$f_2 = 48.339$	$f_1 = 10.986$	$f_2 = 32.684$
Damping ratio	1.0397	0.8211	1.2985	0.2889

In the finite element model, modulus of elasticity for the beam and column used in the steel frame is 2.06×10^6 Mpa. Modulus of elasticity for prefabricated hanger column is 2.55×10^4 Mpa. The moment of inertia for beam and column is $I_x = 847\,\text{cm}^4$ and $I_y = 294\,\text{cm}^4$. Besides, the moment of inertia for prefabricated hanger column is $I_x = 96\,\text{cm}^4$ and $I_y = 1944\,\text{cm}^4$. Moreover, it is considered that the bottom of the finite element model is embedded in the ground. During the analysis of dynamic property for the finite element model, the following are consistent with the actual conditions for the experimental model: (1) earthquake fortification is of C-class; (2) seismic precautionary intensity is 8 degrees (0.2 g); (3) site condition belongs to category II; (4) classification of design earthquake in Chinese Code for seismic design of buildings is first group; (5) ground roughness belongs to category B; (6) basic wind pressure is $0.4\,\text{kN/m}^2$; (7) damping ratio of the experimental model is 1.0397.

4.2. Verification of Finite Element Model. In order to obtain the suitable magnification factor of stiffness for prefabricated hanger column, the magnification factor is set to be 1.0, 1.1, and 1.2, respectively. Natural frequencies for the finite element model can be determined with the eigenvector method, as shown in Table 3.

As can be seen from Table 3, it indicates that with increasing of magnification factor, natural frequency for the finite element model also increases. Compared with Table 1, when the magnification factor of stiffness is 1.2, natural frequency obtained with the finite element method is in good agreement with that obtained with the forced vibration method. When the magnification factor of stiffness is 1.2, the difference between natural frequencies obtained with the forced vibration method and with the finite element method in second-order vibration mode is larger than that in first-order vibration mode, as shown in Table 4.

Based on the finite element method, vibration modes of experiment model in X direction can be determined, as shown in Figures 21(a) and 21(b). Besides, vibration modes of experiment model in Y direction can also be determined, as shown in Figures 21(c) and 21(d). In Figures 21(a) and 21(b), vibration modes in X direction, obtained with the forced vibration method, are also shown. In addition, vibration modes in Y direction, obtained with the forced vibration method, are shown in Figures 21(c) and 21(d).

As can be seen from Figures 21(a)–21(d), vibration modes obtained with the finite element method are rather in agreement with that obtained with the forced vibration

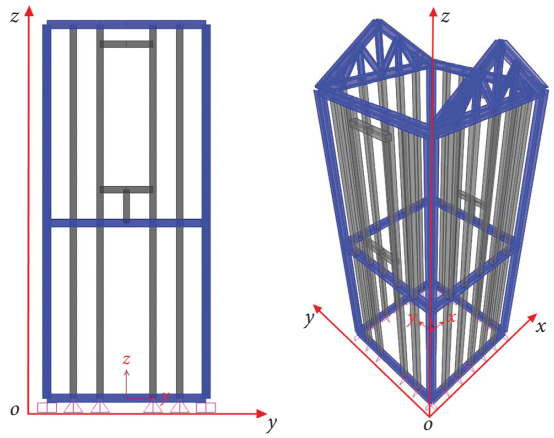

(a) (b)

Figure 20: Finite element model. (a) In plan of *Y*-*Z*. (b) In space of *X*-*Y*-*Z*.

Table 3: Natural frequencies obtained with the finite element method.

Vibration mode	Natural frequency in *X* direction (Hz)			Natural frequency in *Y* direction (Hz)		
	Magnification factor of stiffness for prefabricated hanger column					
	1.0	1.1	1.2	1.0	1.1	1.2
First order	10.5626	12.8751	16.9137	8.0154	9.9852	11.0617
Second order	33.2546	40.2262	44.0106	22.4567	26.7878	33.7984

Table 4: Frequency obtained with the forced vibration method and finite element method (Hz).

Vibration mode		Forced vibration method	Finite element method	Difference
In *X* direction	First order	16.724	16.9137	−1.13%
	Second order	48.339	44.0106	8.95%
In *Y* direction	First order	10.986	11.0617	−0.69%
	Second order	32.684	33.7984	−3.41%

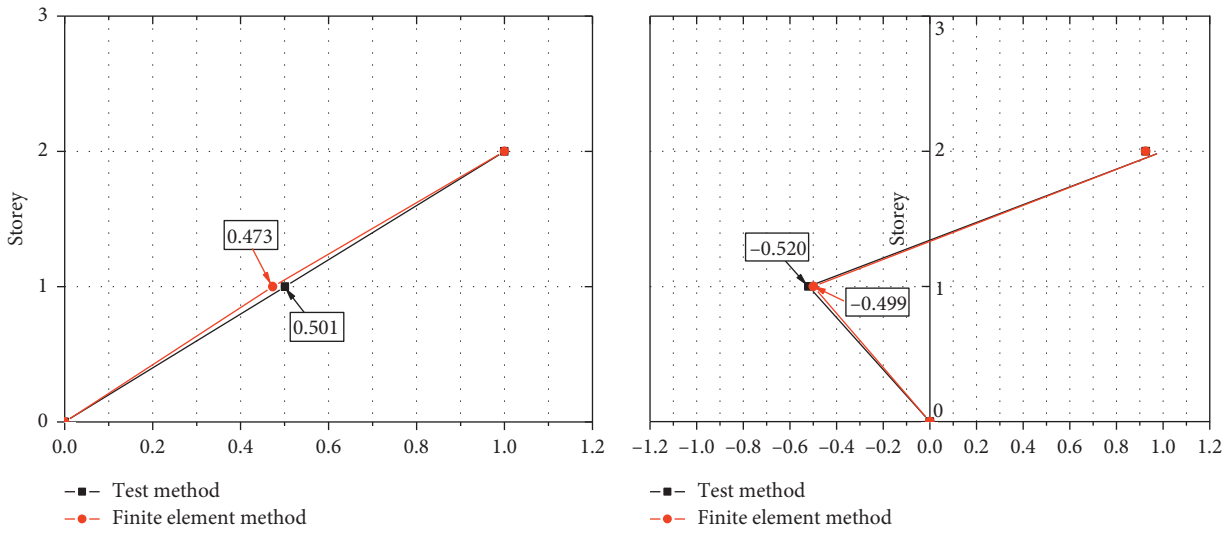

(a) (b)

Figure 21: Continued.

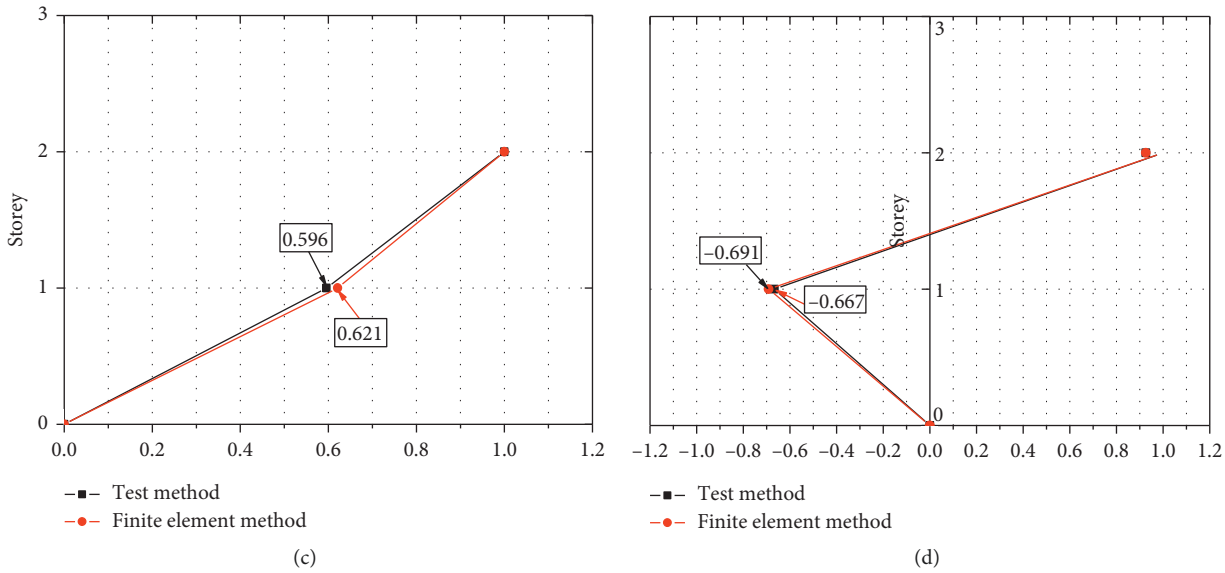

Figure 21: Vibration modes obtained with the forced vibration method and finite element method. (a) First order in X direction. (b) Second order in X direction. (c) First order in Y direction. (d) Second order in Y direction.

Table 5: Participation mass ratio for different modals.

Modal	Frequency (Hz)	Period (s)	UX*	UY	UZ	RX	RY	RZ
First order	11.062	0.091	0	0.78	0	0.91	0	0.240
Second order	15.578	0.064	0.73	0	0	0	0.81	0.220
Third order	18.612	0.054	0	0	0	0	0	0.300

*UX, UY, and UZ: participation mass ratios along X-axis, Y-axis, and Z-axis, respectively; RX, RY, and RZ: participation mass ratios around X-axis, Y-axis, and Z-axis, respectively.

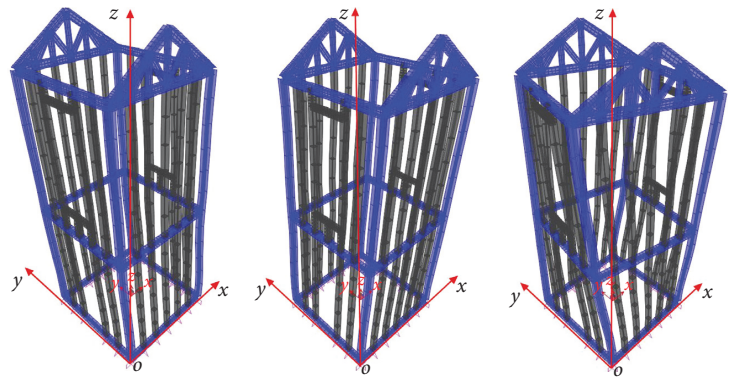

Figure 22: Modal for the experimental model. (a) First-order modal. (b) Second-order modal. (c) Third-order modal.

method. Thus, the finite element model can be applied to study the modal of the experimental model.

4.3. Analysis of Modal. Based on the finite element model with magnification factor of stiffness for prefabricated hanger column 1.2, the improved Ritz vector method is used to obtain the modal for the experimental model. In addition, the method of defining weight including dead load, live load, additional weight, etc., is used in the dynamic analysis of the finite element model. In the finite element model, the number of vibration mode is 3 and frequency deviation is not considered.

Moreover, the participation mass ratios for the experimental model can be determined according to the finite element analysis, as shown in Table 5. Besides, based on the participation mass ratios, the modals of the experimental model at first three modals can also be determined, as shown in Figures 22(a)–22(c), respectively.

For the finite element model, the modal mainly depends on UX, UY, and RZ [25]. If RZ < (UZ + UY), translation modal is dominated in all modals; if RZ > (UX + UY), torsion modal is dominated in all modals. As can be seen from Table 5, for the first-order modal, due to RZ < (UX + UY) and UX < UY, translation modal in Y direction is dominated and torsion modal around Z-axis also exists. For the second-order modal, due to RZ < (UX + UY) and UX > UY, translation modal in X direction is dominated and torsion modal around Z-axis also exists. For the third-order modal, due to RZ > (UX + UY), torsion modal around Z-axis is dominated; however, translation modal in all directions does not exist.

The period of third-order modal is 0.054 s, i.e., $T_t = 0.054$ s, denoting the period of torsion, and the period of first-order modal is 0.091 s, i.e., $T_1 = 0.091$ s, denoting the maximum period of translation. Because $T_t/T_1 = 0.054/0.091 = 0.59$, it is less than 0.9 which is specified by China Code for Seismic Design of Buildings [24]. Therefore, the experimental model can satisfy the requirement of design for seismic performance.

5. Conclusion

In this paper, the dynamic property of a new type of postearthquake temporary prefabricated lightweight steel structure is studied with the test method and finite element method, and the following results are given below:

(i) The united method, proposed based on the forced vibration method and ambient random vibration method, can be used to quickly obtain accurate natural frequencies of the experimental model.

(ii) For first-order vibration mode, damping ratio decreases with increasing of natural frequency, and damping ratio in X and Y direction is 1.0397% and 1.2985%, respectively, which is less than allowable value of 5% required by China Code for Seismic Design of Building.

(iii) When the magnification factor of stiffness for prefabricated hanger column is the value of 1.2 in the finite element model, natural frequencies obtained with the finite element method are in good agreement with that obtained with the test method.

(iv) For the experimental model, due to $T_t/T_1 < 0.9$, it can satisfy the requirement of design for seismic performance.

Data Availability

All the data in this paper are obtained from tests and numerical analysis in this study, and no other data in the literature are used to support this study.

Conflicts of Interest

The authors declare that there are no potential conflicts of interest with respect to the research, authorship, and publication of this article.

Acknowledgments

This study was financially supported by a project of Shandong Province Higher Educational Science and Technology Program (grant no. J17KB059) and Doctoral Scientific Fund Project of Weifang University (grant no. 2017BS14).

References

[1] H. Yin and G. Shi, "Finite element analysis on the seismic behavior of fully prefabricated steel frames," *Engineering Structures*, vol. 173, pp. 28–51, 2018.

[2] X. C. Liu, Z. W. Yang, H. X. Wang et al., "Seismic performance of H-section beam to HSS column connection in prefabricated structures," *Journal of Constructional Steel Research*, vol. 138, pp. 1–16, 2017.

[3] H. M. Xu, Y. Y. Li, and W. Xu, "Dynamic characteristic analysis of prefabricated houses of light-weight steel structure," *Applied Mechanics and Materials*, vol. 578-579, pp. 483–487, 2014.

[4] D. K. Miller, "Lessons learned from the Northridge earthquake," *Engineering Structures*, vol. 20, no. 4–6, pp. 249–260, 1998.

[5] M. Nakashima, K. Inoue, and M. Tada, "Classification of damage to steel buildings observed in the 1995 Hyogoken-Nanbu earthquake," *Engineering Structures*, vol. 20, no. 4–6, pp. 271–281, 1998.

[6] E. P. Popov, T. Yang, and S. Chang, "Design of steel MRF connections before and after 1994 Northridge earthquake," *Engineering Structures*, vol. 20, no. 12, pp. 1030–1038, 1998.

[7] S.-J. Chen, C. H. Yeh, and J. M. Chu, "Ductile steel beam-to-column connections for seismic resistance," *Journal of Structural Engineering*, vol. 122, no. 11, pp. 1292–1299, 1996.

[8] Z. F. Li, Y. J. Shi, H. Chen et al., "Nonlinear element analysis of improved beamcolumn joint of steel structure," *Building Structure*, vol. 32, no. 9, pp. 15–18, 2002, in Chinese.

[9] D. W. Zhao, Y. J. Shi, and H. Chen, "Experimental study of beam-column joint under low cycling load," *Building Structure*, vol. 30, no. 9, pp. 3–7, 2000, in Chinese.

[10] S. C. Goel, S. Leelataviwat, and B. Stojadinovic, "Steel moment frames with ductile girder web opening," *Engineering Journal*, vol. 34, no. 4, pp. 115–125, 1997.

[11] J. A. Swanson and R. T. Leon, "Bolted steel connections: tests on t-stub components," *Journal of Structural Engineering*, vol. 126, no. 1, pp. 50–56, 2000.

[12] Y. Harada and K. Morita, "Design of wide-flange section column-to-split-tee tensile connection with high-strength bolts," *Journal of Structural Engineering*, vol. 133, no. 1, pp. 335–346, 2007.

[13] V. Piluso and G. Rizzano, "Experimental analysis and modelling of bolted T-stubs under cyclic loads," *Journal of Constructional Steel Research*, vol. 64, no. 6, pp. 655–669, 2008.

[14] E. P. Popov and S. M. Takhirov, "Bolted large seismic steel beam-to-column connections Part 1: experimental study," *Engineering Structures*, vol. 24, no. 12, pp. 1523–1534, 2002.

[15] J. Lee, H. M. Goldsworthy, and E. F. Gad, "Blind bolted moment connection to unfilled hollow section columns using extended T-stub with back face support," *Engineering Structures*, vol. 33, no. 5, pp. 1710–1722, 2011.

[16] A. L. Zhang, L. Zhao, and X. C. Liu, "Monotonic experimental study of prefabricated square tubular column to truss beam connections," *China Civil Engineering Journal*, vol. 47, no. 2, pp. 169–174, 2014, in Chinese.

[17] X. C. Liu, A. X. Xu, A. L. Zhang et al., "Static and seismic experiment for welded joints in modularized prefabricated steel structure," *Journal of Constructional Steel Research*, vol. 138, no. 15, pp. 1–16, 2017.

[18] X. C. Liu, S. H. Pu, A. L. Zhang et al., "Static and seismic experiment for bolted-welded joint in modularized prefabricated steel structure," *Journal of Constructional Steel Research*, vol. 115, pp. 417–433, 2015.

[19] X. C. Liu, S. H. Pu, A. X. Xu et al., "Experimental study on static and seismic performance of bolted joint in modularized multi-layer and high-rise prefabricated steel structures," *Journal of Building Structures*, vol. 36, no. 12, pp. 43–51, 2015, in Chinese.

[20] Q. S. Li, J. Q. Fang, and A. P. Jeary, "Free vibration analysis of cantilevered tall structures under various axial loads," *Engineering Structures*, vol. 22, pp. 525–534, 2000.

[21] R. Yoshie, H. Kawai, M. Shimura, and R. Wei, "A study on wind-induced vibration of super high rise building by multi-degree-of freedom model," *Journal of Wind Engineering and Industrial Aerodynamics*, vol. 69-71, pp. 745–755, 1997.

[22] S. M. J. Spence, E. Bernardini, Y. Guo, A. Kareem, and M. Gioffrè, "Natural frequency coalescing and amplitude dependent damping in the wind-excited response of tall buildings," *Probabilistic Engineering Mechanics*, vol. 35, pp. 108–117, 2014.

[23] L. Hermans and H. Van Der Auweraer, "Modal testing and analysis of structures under operational conditions: industrial applications," *Mechanical Systems and Signal Processing*, vol. 13, no. 2, pp. 193–216, 1999.

[24] GB 50011-2010, *Code for Seismic Design of Buildings*, Ministry of Housing and Urbal-Rural Development of China and General Administration of Quality Supervision, Inspection and Quarantine of China, Beijing, China, 2016.

[25] C. King Infornation Technology Co. Ltd and China Institute of Building Standard Design and Research, *Guideline in chinese for SAP2000*, China Communications Press, Beijing, China, 2006.